BIODIVERSITAS
Volume 25, Number 9, September 2024
Pages: 3189-3200

ISSN: 1412-033X
E-ISSN: 2085-4722
DOI: 10.13057/biodiv/d250941

Satellite remote sensing techniques for mapping and estimating mangrove carbon stocks in the small island of Gili Meno, West Nusa Tenggara, Indonesia

I WAYAN GEDE ASTAWA KARANG[1,♥], I WAYAN NUARSA[1], I GEDE HENDRAWAN[1], NI MADE NIA BUNGA SURYA DEWI[2], PUTU KUMARA YASA[1], I MADE DWITA KRISNANDA[1]

[1]Department of Marine Sciences, Faculty of Marine Science and Fisheries, Universitas Udayana. Jl. Kampus Bukit Jimbaran, South Kuta 80361, Badung, Bali, Indonesia. Tel./Fax. +62-361-702802, ♥email: gedekarang@unud.ac.id

[2]Doctoral Program of Environmental Science, Universitas Udayana. Jl. Panglima Besar Sudirman, Denpasar 80234, Bali, Indonesia

Manuscript received: 17 June 2024. Revision accepted: 21 September 2024.

Abstract. *Karang IWGA, Nuarsa IW, Hendrawan IG, Dewi NMNBS, Yasa PK, Krisnanda IMD. 2024. Satellite remote sensing techniques for mapping and estimating mangrove carbon stocks in the small island of Gili Meno, West Nusa Tenggara, Indonesia. Biodiversitas 25: 3189-3200.* Estimating mangrove carbon stocks is crucial for effective conservation and management but presents challenging, particularly on small islands. Satellite remote sensing offers a powerful tool for assessing mangrove ecosystems, though its application in small island environments remains underutilized. This study aims to explore and evaluate the effectiveness of satellite remote sensing techniques, specifically using Sentinel-2, for mapping and estimating mangrove carbon stocks on the small island of Gili Meno, West Nusa Tenggara, Indonesia. The Random Forest technique was employed to distinguish between mangrove and non-mangrove areas by analyzing multiple parameters. Additionally, a semi-empirical method was used to evaluate and map the Above Ground Carbon (AGC) of mangroves, with general allometric equations applied to calculate AGC values. Six vegetation indices were assessed to develop a model for estimating mangrove AGC using linear regression equations. The accuracy of the model predictions was evaluated using the Root Mean Square Error. The study identified that the mangrove forest area in Gili Meno covers approximately 6.88 ha. Notably, the research revealed that the IRECI model, with an R^2 value of 0.76 and RMSE of 17.14 ton/ha, was the most effective for AGC estimation when utilizing red edge bands.

Keywords: Above ground carbon, Random Forest, Sentinel-2, small islands, vegetation indices

Abbreviations: AGB: Above Ground Biomass, AGC: Above Ground Carbon, DBH: Diameter at Breast Height, GBH: Girth at Breast Height, GEE: Google Earth Engine, RF: Random Forest, RMSE: Root Mean Square Error

INTRODUCTION

Mangrove forests are essential to coastal communities and are among the world's most diverse ecosystems (Iqbal 2020; Worthington et al. 2020). In recent years, the role of mangrove ecosystems in climate change mitigation and adaptation has gained considerable recognition (Dinilhuda et al. 2020). Mangroves not only provide essential ecological functions and ecosystem services but also play a vital role in carbon sequestration (Murdiyarso et al. 2015). An accurate estimation of mangrove carbon stocks is crucial for understanding their contribution to global carbon budgets and for implementing effective conservation and management strategies (Kristensen et al. 2008; Saragi-Sasmito et al. 2018). However, obtaining precise and up-to-date carbon stock information for mangroves, particularly on small islands, presents a significant challenge.

The challenges in conducting surveys and sampling in mangrove forests include the dense forest conditions that hinder accessibility and were influenced by periodic tidal fluctuations. Recent advancements in remote sensing technology have offered innovative solutions to these challenges, enabling more accurate and efficient assessments of mangrove ecosystems. Satellite remote sensing has emerged as a potent due to its capability to assess and monitor mangrove ecosystems across extensive spatial scales (Giri et al. 2011), enabling researchers to gather valuable information on mangrove extent, structure, and above-ground biomass. Various remote sensing techniques have been developed, including optical methods with different algorithms, each with its strengths and limitations (Zhang and Lin 2014). Numerous studies have employed remote sensing to map above ground carbon in mangroves (Wicaksono et al. 2016; Hickey et al. 2018; Pham et al. 2018; Bindu et al. 2020). However, it was crucial to understand the accuracy of these techniques when applied to mangroves with small area extents, as several issues in mangrove mapping involve the synchronization of field data with remote sensing approaches, requiring specific adjustments.

Sentinel-2 mission fouses on high-resolution multispectral imaging for global land observation. Each satellite in this mission is equipped with a Multispectral Instrument (MSI) featuring a wide swath width of 290 km and a high revisit frequency. What sets Sentinel-2 MSI apart from other multispectral sensors is its ability to provide three spectral bands within the red-edge range,

making it particulary valuable for vegetation monitoring (She et al. 2020). Sentinel image analysis, using the Normalized Difference Vegetation Index (NDVI), Soil Adjusted Vegetation Index (SAVI), and Normalised Difference Water Index (NDWI), effectively identifies density of mangrove vegetation. The NDVI transformation highlights high-density classes, while the SAVI transformation emphasize very low-density class, and the NDWI transformation is dominated by low-density classes. An accuracy test conducted on these transformations yielded accuracy of 83.33% (Simarmata et al. 2021). Additionally, the Mangrove Vegetation Index (MVI) demonstrated an overall index accuracy of 92% using Sentinel-2 imagery (Baloloy 2020).

Gili Meno, a small island located in Gili Indah Village, Pemenang Sub-district, North Lombok District, West Nusa Tenggara Province, Indonesia. Having coral reefs, seagrass beds, mangroves, and other marine life, the island holds significant potential for biodiversity research and marine tourism (Rahman and Hadi 2021). Gili Meno exhibits unique mangrove characteristics, with mangroves encircling a saltwater lake and grows alongside other tropical plants. These unique characteristics poses a challenge for remote sensing applications, particularly in assessing the accuracy of remote sensing techniques when applied to small mangroves areas. Identifying individual trees become difficult when their canopies are smaller than the image resolution, especially in mixed communities or dense areas where closely related species exhibit similar spectral reflectance (Maurya et al. 2021).

This study aimed to explore and evaluate the effectiveness of satellite remote sensing techniques for mapping and estimating mangrove carbon stocks on the small island of Gili Meno. Given the unique characteristics of the mangrove ecosystems in this area, particularly the presence of mangrove encircled saltwater lake, understanding the accuracy of remote sensing applications becomes imperative. In summary, the study assessed the application of satellite remote sensing in mapping and estimating mangrove carbon stocks in Gili Meno, considering the unique characteristics of the mangrove ecosystems in this small island setting. The findings are expected to contribute valuable information for both scientific understanding and practical conservation efforts in mangrove-rich coastal areas.

MATERIALS AND METHODS

Study area

This research was conducted in September 2023 at the Aquatic Tourism Park (ATP) in Gili Meno, West Nusa Tenggara Indonesia as shown in Figure 1. Geographically, Gili Meno is located between 8°20'-8°23'S latitude and 116°00'-116°08'E longitude. The island covers an area of approximately 150 hectares and features a mangrove region located on the western side, along the coastline, surrounding a saltwater lake. The ecosystems within ATP Gili Meno consist of seagrass beds and mangrove forests, with a potential mangrove area of 1.81 hectares. This area is home to eight species of mangrove trees belonging to eight different families, including *Bruguiera cylindrica*, *Sonneratia alba*, *Avicennia alba*, *Lumnitzera racemosa*, *Excoecaria agallocha*, *Pemphis acidula*, *Acrostichum aureum* and *Cynometra* sp. Generally, the mangroves grow in clumps that are separated and mixed with coastal plants. The *P. acidula* (locally called *centigi*) is a type of mangrove that predominantly grows along the beach (KKP 2020).

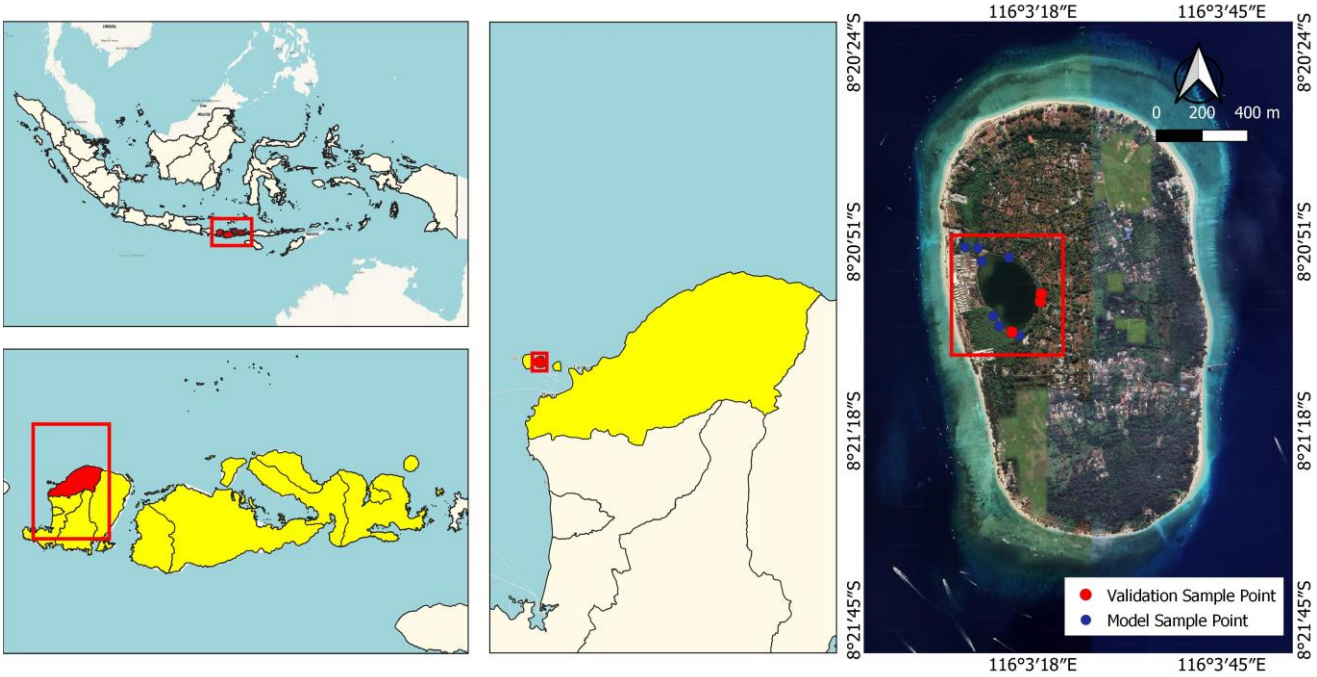

Figure 1. Study area in Gili Meno, West Nusa Tenggara, Indonesia

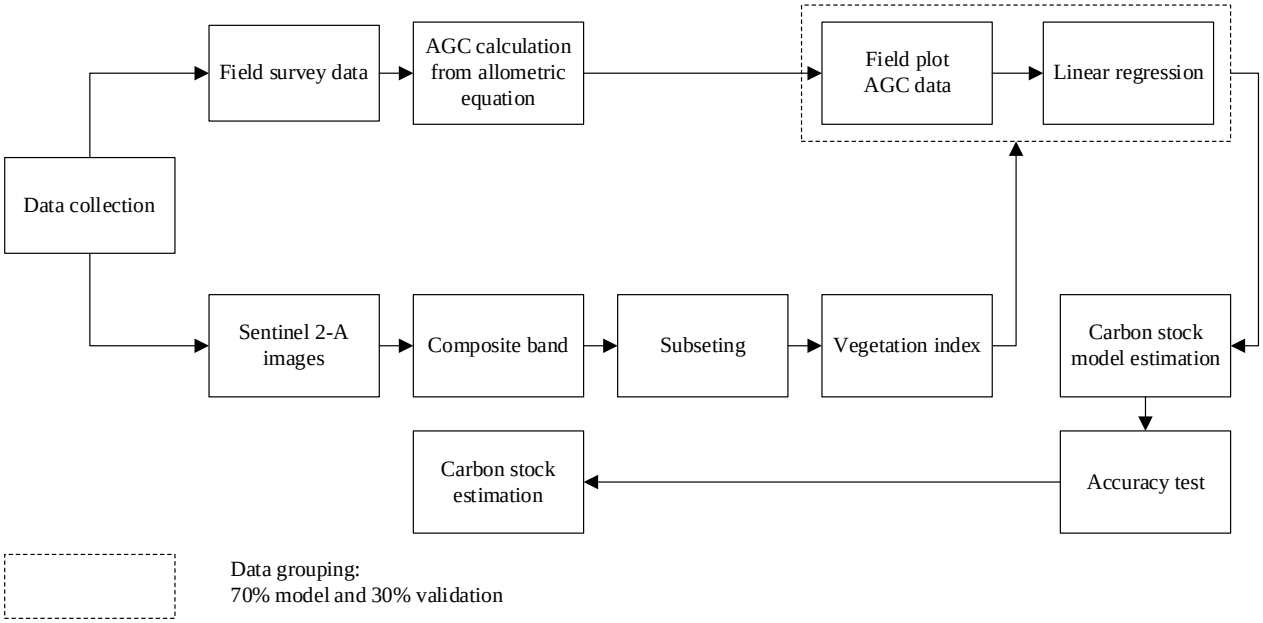

Figure 2. The flowchart of the methodologies employed in the study for the mapping and computation of Aboveground Carbon (AGC) in mangrove

Methods

The methodological scheme used for estimating Above Ground Biomass model using Sentinel 2 imagery is presented in Figure 2.

Field data collection

This study was conducted at the Aquatic Tourism Park (ATP) in Gili Meno, West Nusa Tenggara, Indonesia. Field data collection was conducted from 8th to 10th September, 2023, a period chosen for its dry weather conditions to avoid constraints posed by rain during field activities. A total of 10 field points were established, with seven points (70%) allocated for model construction and three points (30%) for model validation. The selection of these field points employed a random sampling method, tailored to the accessibility of each location. Each point was demarcated by plots measuring 10×10 m^2 (Figure 3). The transect line employed in this study was adapted from Kauffman and Donato (2012), with shape modified from circular to square to better align with the pixel structure of remote sensing imagery.

Mangrove measurements were conducted within predetermined field plots. For upright mangroves, it was assumed that the trees have a circular shape, and both the circumference and diameter were measured. The stem circumference was measured at breast height, defined as 1.3 meters above the ground, which corresponds to the average height of an adult (Figure 4). This measurement is referred to as the Girth at Breast Height (GBH). To convert the GBH value to Diameter at Breast Height (DBH), a general formula for calculating the diameter from a circle's circumference was applied using the equation DBH = GBH/π, where π is a constant value of 3.14. DBH measurements were carried out within the established plots, focusing specifically on tree stems with a diameter below 5 cm and a height exceeding 1.5 m, as well as on tree stems with a diameter equal to or greater than 5 cm.

Data processing

Pre-processing

The initial stage in satellite image processing involves pre-processing of the imagery. This research considered various key aspects, including the importing of image data, resampling, image subsetting, and selecting of a composite band.

Processing

The Sentinel-2 image data used in this study were obtained from the Google Earth Engine (GEE) collection datasets and processed using JavaScript programming within the GEE environment. The data spanned from 1st September to 30th September, 2023, focusing on Sentinel-2 Level-2A imagery with atmospherically corrected Surface Reflectance (SR) and less than 20% cloud cover. This selection criteria ensured the creation of a composite image free from clouds over the entire study area and its surrounding regions. Cloud masking was performed using a combination of the Quality Assessment (QA) band and the median reducer function available in GEE. The QA band was employed to remove cloud contamination within each image, while the median reducer function enabled the extraction of the mean pixel value across the entire image stack, resulting in an image devoid of overly bright (e.g., clouds) or dark (e.g., shadows) pixel values.

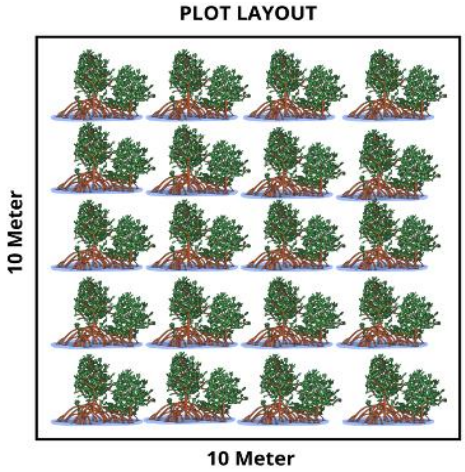

Figure 3. Illustration of plot layout for field measurement

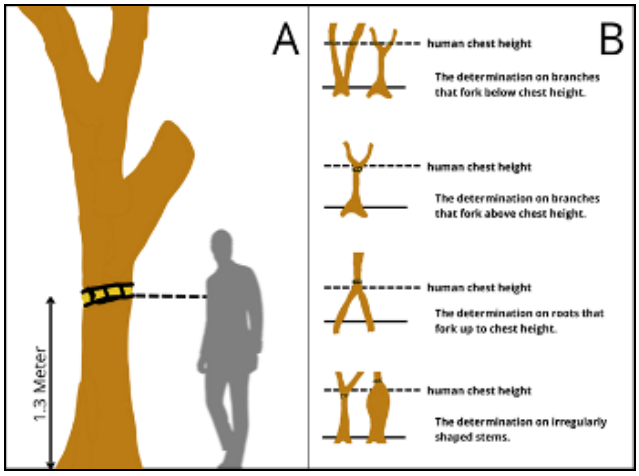

Figure 4. Mangrove DBH measurement technique

The classification of mangrove and non-mangrove was conducted using the Random Forest (RF) classification method on the GEE platform. This approach divided the study area into two distinct land covers, based on visual interpretations of false-color images, utilizing bands such as Near-Infrared (NIR), Short-Wave Infrared (SWIR), and Red. The RF algorithm, known for its effectiveness in classification and regression tasks (Akhiat et al. 2021), was selected for this study. It achieves robustness by combining predictions from multiple decision trees, each trained on different data subsets. The RF algorithm's ability to estimate the relative importance of each input feature, facilitated feature selection and enhanced understanding of the underlying factors influencing outcomes.

Calculation of vegetation indices

Six vegetation indices, were used to develop the estimation model for above-ground mangrove carbon stock (Table 1). These indices include NDVI, Modified Red Edge-Simple Ratio (mRE-SR), Total Ratio Vegetation Index (TRVI), Inverted Red-edge Chlorophyll Index (IRECI), Red-edge Chlorophyll Index (CIR), and Optimized Soil Adjusted Vegetation Index (OSAVI).

Above ground biomass and above ground carbon

The estimation of mangrove carbon was based on Above Ground Biomass (AGB) values. Before determining the Above Ground Carbon (AGC) values, the AGB of mangroves was calculated for each species encountered using a general allometric equation specifically tailored for Asian mangroves, ensuring its applicability in Indonesia. Allometric equations are crucial for estimating mangrove biomass based on the Diameter at Breast Height (DBH) parameter (Kumar and Mutanga 2017). The general mangrove allometric equation employed in this study is expressed as $W_{top} = 0.251 \times p \times DBH^{2.46}$ (Komiyama et al. 2005) where p = wood density (Table 2).

Table 1. Equations for the vegetation indices used in development of the above-ground mangrove carbon stock model

Vegetation indices	Equations	Sources
NDVI (Normalized Difference Vegetation Index)	$NDVI = \frac{\text{Band 8} - \text{Band 4}}{\text{Band 8} + \text{Band 4}}$	Rouse et al. (1973) Ramdani et al. (2018)
mRE-SR (Modified Red Edge – Simple Ratio)	$mRE - SR = \frac{\left(\frac{Band\ 8}{Band\ 5}\right) - 1}{\sqrt{\left(\frac{Band\ 8}{Band\ 5}\right) + 1}}$	Zhu et al. (2017) Wahyuni et al. (2024)
TRVI (Total Ratio Vegetation Index)	$TVRI = \sqrt{\frac{Band\ 8}{Band\ 4}}$	Fadaei et al. (2012) As-syakur et al. (2023)
IRECI (Inverted Red-edge Chlorophyll Index)	$IRECI = \frac{\text{Band 8} - \text{band 4}}{\frac{Band\ 5}{Band\ 6}}$	Blackburn (1998) Alam et al. (2017)
CIR (Red-edge Chlorophyll Index)	$CIR = \frac{\text{Band 7}}{\text{Band 5}} - 1$	Gitelson et al. (2003) Zheng et al. (2018)
OSAVI (Optimized Soil Adjusted Vegetation Index)	$OSAVI = \frac{1.5\ \text{x}\ (\text{Band 8} - \text{Band 4})}{(\text{Band 8} + \text{Band 4} + 0.16)}$	Rondeaux et al. (1996) Liu et al. (2020)

Table 2. Wood density of some mangrove species

Mangrove species	Wood density (g/cm^3)
Avicennia marina	0.7316
Bruguiera cylindrica	0.8100
Lumnitzera racemosa	0.8325
Rhizophora apiculata	0.8814

Source: World Agroforestry Center (2022)

The AGC was derived from AGB based on the guidelines outlined in the Indonesian National Standard (2011) 7724:2011, which states that 47% of the biomass consists of carbon. The calculation of AGC followed the approach proposed by Fourqurean et al. (2019), using the equation:

$$AGC=AGB\times 0.47$$

Data analysis

Simple linear regression

Simple Linear Regression (SLR) analysis was used to build a linear model for estimating AGC in mangroves. The regression coefficient measured the magnitude of the effect of vegetation index (X) value on the dependent variable (Y), which is the ground truth carbon value, within the linear regression equation model. The regression equation is represented as follows:

$$Y = a + bX$$

$$b = \frac{n\,(\sum xy) - (\sum x).(\sum y)}{n\,(\sum x^2) - (\sum x)^2} a + bX$$

$$a = \frac{\sum y - b - (\sum x)}{n}$$

Where, X represents the vegetation index value, Y represents the ground truth carbon value, a is a constant, b is the regression coefficient, and n represents the number of data points.

Model validation

Validation tests were conducted to assess discrepancies in the estimated carbon stock values in mangroves derived from the constructed regression models. The model validation involved comparing the diameter values obtained from field plots with those linear model equation applied to the Sentinel 2-A image for each vegetation index. The accuracy of the model was evaluated using Root Mean Square Error (RSME), while the coefficient of determination (R^2) served as a metric for assessing the model's accuracy. The field data were used to validate the AGC outcomes generated by the model, with error values calculated using the RMSE, as shown in the following equation:

$$RMSE = \frac{\sqrt{\sum (E-0)^2}}{n}$$

RESULTS AND DISCUSSION

Mangrove species identification

Based on observational data, mangroves in Gili Meno were identified as belonging to three families: Acanthaceae, Combretaceae, and Rhizophoraceae, comprising four species. The order of mangrove species from most to least common was *Avicenia marina* > *B. cylindrica* > *L. racemosa* > *Rhizophora apiculata* (Figure 5). *Avicennia marina*, the most frequently found species in Gili Meno, is known for its adaptibility to saline and muddy environmental conditions. The substrate in every research plot was observed to be muddy. The DBH size varied, ranging from 1.3 cm (*A. marina*) to 28.3 cm (*A. marina*). The *A. marina*, the dominant species, had the highest average DBH at 8.8 cm.

Image classification and extraction of mangrove forests

Figure 6 presents the results of image pre-processing, including sub-setting and creating a composite image. The composite image was used to differentiate between mangrove and non-mangrove areas, utilizing a false-color RGB composite (NIR, SWIR, Red) image. Based on the composite image results, mangrove objects and natural vegetation exhibited similar colors and were found in close proximity to each other. Mangroves were identified by their bright red color, while regular vegetation appeared a slightly darker red.

Avicennia marina *Lumnitzera racemosa* *Bruguiera cylindrica* *Rhizophora apiculata*

Figure 5. Four mangrove species in Gili Meno, West Nusa Tenggara, Indonesia

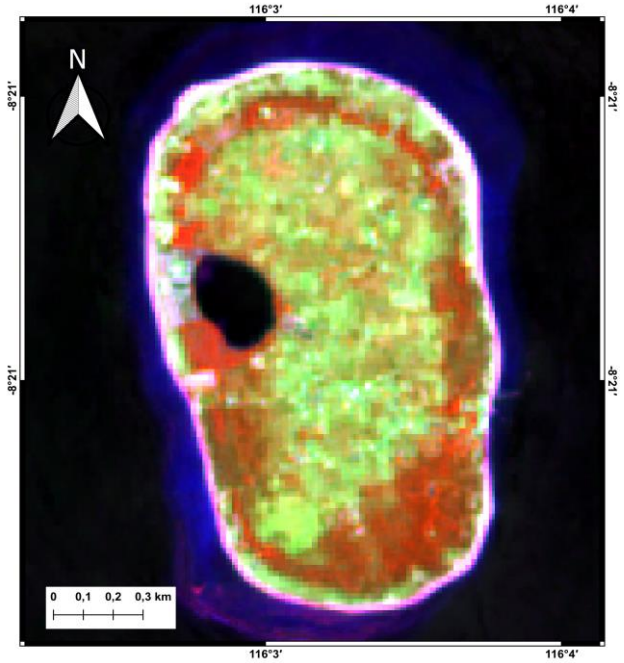

Figure 6. Sentinel-2 composite RGB false colour (NIR, SWIR, Red)

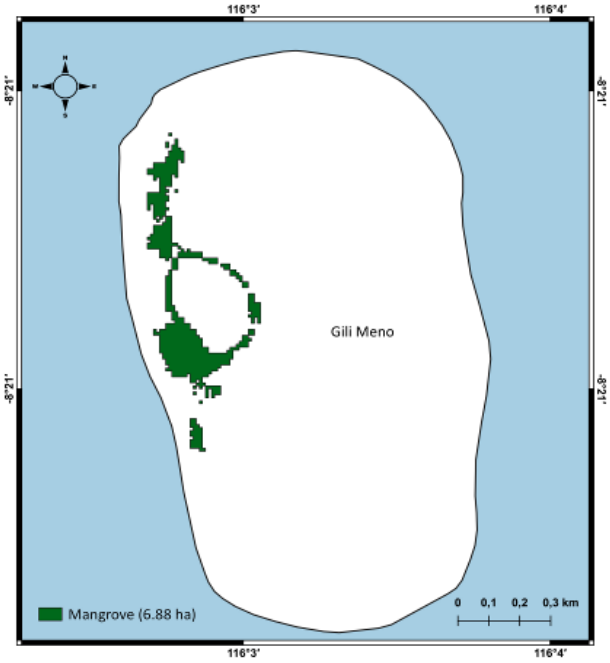

Figure 7. The mangrove area in Gili Meno, West Nusa Tenggara, Indonesia, is classified using RF methods

The mangrove area within the research site on Gili Meno was estimated to be approximately 6.88 hectares (Figure 7). The Random Forest (RF) method was employed to classify mangrove and non-mangrove areas using various parameters, resulting in high accuracy, with an Overall Accuracy (OA) of 0.91 and a kappa coefficient value of 0.9. The classification results derived from Sentinel-2 imagery showed significant agreement with the field data, as reflected in the kappa coefficient (Dan et al. 2016). The high classification accuracy can be attributed to several factors, including the use of limited classes (mangrove and non-mangrove), uniform sample point determination (Dong et al. 2020), and careful consideration of tidal duration, and cloud cover percentage (Dong et al. 2020). Additionally, including multiple parameters that are highly sensitivity to mangrove forest detection in the RF classification process has been demonstrated to enhance classification accuracy.

Above ground carbon

Ground truth data collected on 9th September, 2023, in Gili Meno revealed that point 7 had the highest AGC value, at 190.40 tons per hectare, while point 1 recorded the lowest AGC value of 41.20 tons per hectare (Table 3). The average AGC across the 10 plots was calculated to be 103.16 tons per hectare. The AGC estimation model was developed based on the assumption that AGB is closely associated with tree diameter (DBH) and wood density. AGB significantly influenced the amount of AGC stored within each tree, demonstrating a positive correlation between biomass increment and carbon accumulation (Purnamasari et al. 2021).

The dominant species in the study area were identified as *A. marina*, which coincidentally exhibited the highest AGC values at the dominant sample points. The carbon stock within mangrove stands was notably influenced by variables such as DBH, canopy cover and biomass density (Suwa et al. 2021)

Relationship between observed AGC and Sentinel-2 derived vegetation indices

The relationship between field-observed AGC and several vegetation indices is depicted in Figure 8. The selected vegetation indices were based on the red edge and Near-Infrared (NIR) bands, known for their sensitivity in vegetation detection (Nguy-Robertson et al. 2014; Imran et al. 2020). Among the examined vegetation indices, the IRECI index demonstrated the highest performance, with an R^2 value of 0.76 and an associated error of 17.14 tons per hectare. Importantly, all the vegetation indices were able to explaining a significant portion of the data variance, with R^2 values exceeding 0.70 (Table 4).

Table 3. Results of biomass and carbon stock calculation in Gili Meno, West Nusa Tenggara, Indonesia

Sample point	AGB (ton/ha)	AGC (ton/ha)	Dominant spesies
1	87.72	41.23	*A. marina*
2	199.14	93.59	*A. marina*
3	270.72	127.24	*A. marina*
4	149.76	70.39	*A. marina*
5	125.77	59.11	*A. marina*
6	299.26	140.65	*A. marina*
7	405.12	190.40	*A. marina*
8	170.71	80.23	*A. marina*
9	264.26	124.20	*A. marina*
10	222.52	104.58	*A. marina*

In this research, the model was constructed by vegetation indices to minimize prediction error. The selection of vegetation indices was based on those incorporating red edge bands as well as those that excluded them. Figure 9 illustrates the linear regression between observed carbon and the selected vegetation indices.

Relationship between ground truth AGC and spectral reflectance

The relationship between Sentinel-2 multispectral bands and AGC ground truth is presented in Table 5. The Red edge 2, Red edge 3, and NIR bands showed a strong correlation with AGC, with R^2 values of 0.59, 0.60, and 0.66, respectively, and error prediction values of 24.30, 23.21, and 30.50. These findings indicate that these bands significantly contribute to explaining data variation. Conversely, the blue, red, and SWIR bands exhibited a weak relationship with AGC, while the Green and Red edge 1 bands have a very weak correlation.

Mangrove carbon predictive mapping

The model that employed the most optimal algorithm, characterized by the highest R^2 value and lowest standard error and RMSE, was utilized to estimate and map AGC values across the research area. The equation representing the model with the superior algorithm is displayed below.

$$AGC = -7.5811 + 354,95 * IRECI$$

Figure 11 illustrates the spatial distribution of AGC estimated using the IRECI index. The accuracy evaluation of the Sentinel-2-based AGC prediction maps showed that the prediction error (RMSE) value for IRECI ranged from 17.14 ton/ha. The coefficient of agreement (r) and coefficient of determination (R^2) between the measured and predicted carbon were calculated at 0.87 and 0.76, respectively, for IRECI. The predicted AGC based on the best indices indicates that mangrove in Gili Meno has an average AGC value of 99.85 ton/ha, leading to an estimated total AGC in Gili Meno of 687.96 ton.

Table 4. Correlation of AGC and vegetation indices

Indices	r	R2	RMSE (±ton/ha)	Standard Error
NDVI	0.85	0.73	26.06	29.89
mRE-SR	0.84	0.71	31.09	31.02
TRVI	0.87	0.76	26.00	27.96
IRECI	0.87	0.76	17.14	28.07
CIR	0.84	0.71	11.98	30.97
OSAVI	0.86	0.73	21.04	29.81

Table 5. Correlation of ground truth AGC with spectral reflectance

Indices	r	R^2	RMSE (±Ton/Ha)	Standard Error
Blue	0.60	0.35	42.10	46.20
Green	0.13	0.02	16.21	57.00
Red	0.56	0.31	43.04	47.68
Red edge 1	0.25	0.06	25.17	55.75
Red edge 2	0.77	0.59	24.30	36.99
Red edge 3	0.77	0.60	23.21	36.43
NIR	0.81	0.66	30.50	33.70
SWIR	0.60	0.36	18.30	46.15

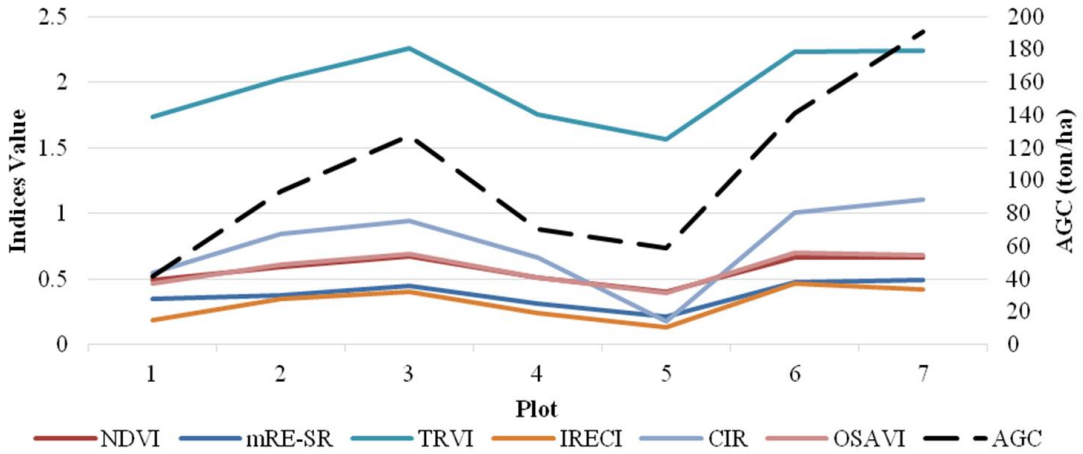

Figure 8. Relationship between observed AGC and Sentinel-2 derived vegetation indices. Plots were organized based on carbon levels, ranging from nil to high

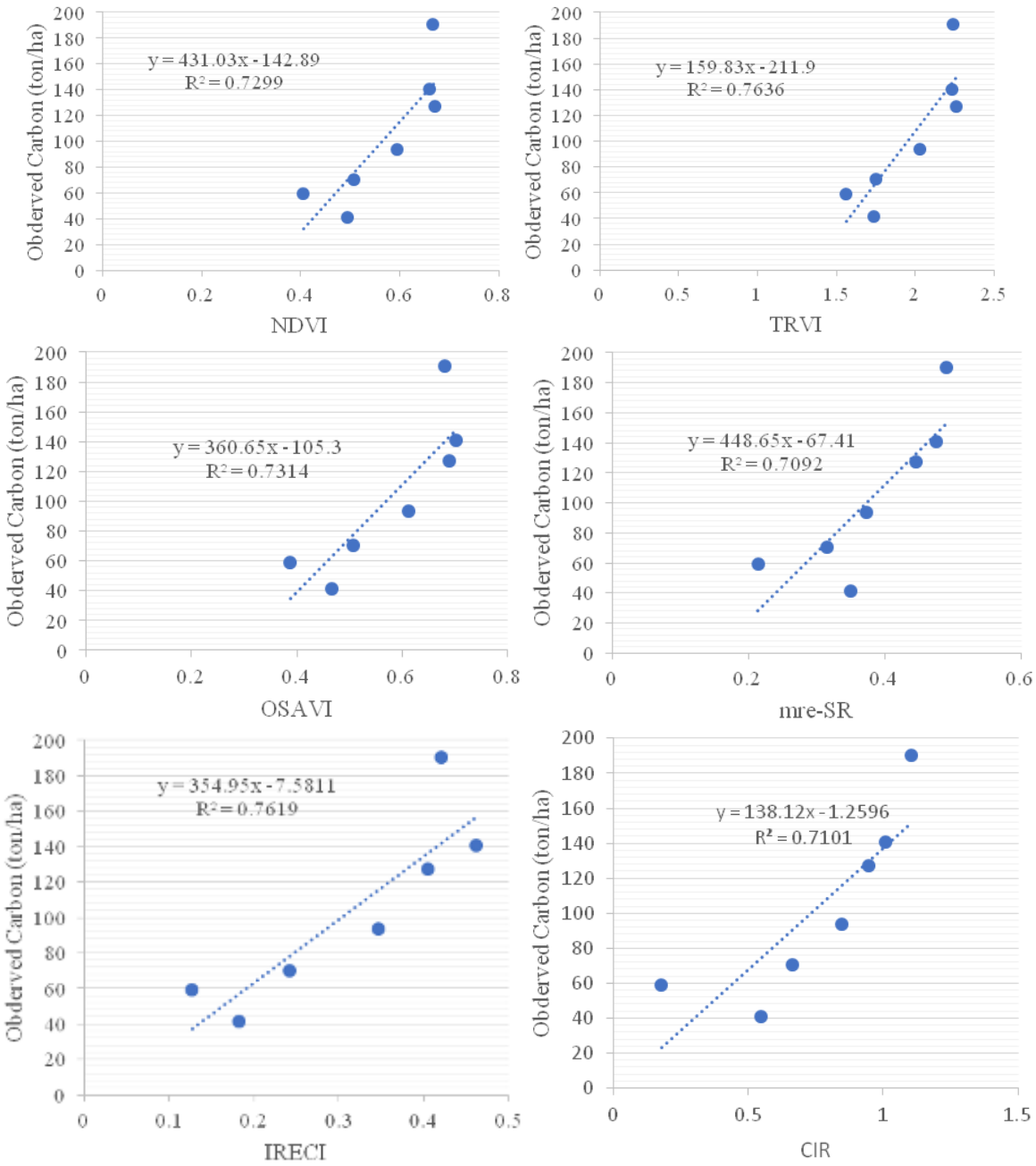

Figure 9. Linear regression of observed carbon and vegetation indices

Figure 10. Evidence of spot logging in the mangrove areas of Gili Meno, West Nusa Tenggara, Indonesia

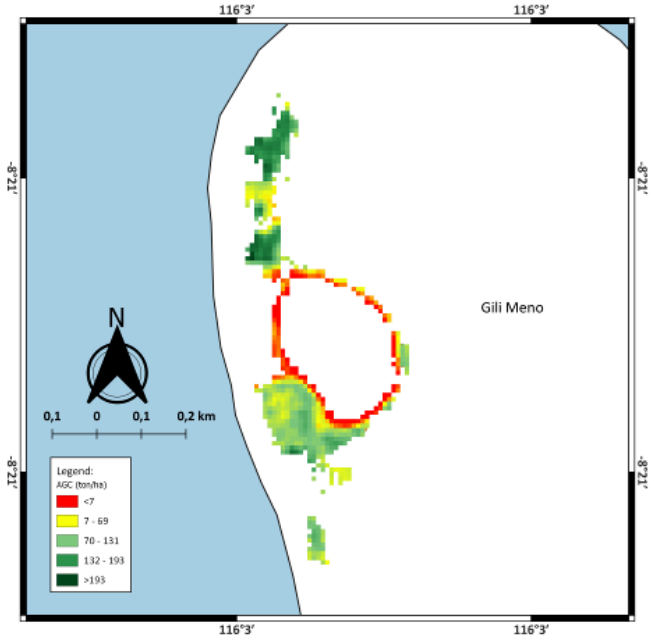

Figure 11. Carbon prediction (ton/ha) using the best correlation equation result in Gili Meno, West Nusa Tenggara, Indonesia

Discussion

Mangroves on Gili Meno Island are currently facing significant challenges, primarily driven by the rapid expansion of the tourism sector. Construction activities near the mangrove areas have led to the substantial loss of mangroves due to logging (Figure 10). Additionally, the mangrove ecosystems in Gili Meno are highly vulnerable to waste accumulation, which is attributed to the proximity of anthropogenic activities to these areas. The presence of debris around the mangrove areas suggests a high potential for pollution from human activities. This study also assessed the substrate conditions within the mangrove area, particularly in the designated research plots. Observations revealed that the substrate in these plots is predominantly composed of sandy mud.

The mangrove species found on Gili Meno Island belong to the families Acanthaceae, Combretaceae, and Rhizophoraceae, comprising of four species: *A. marina*, *L. racemosa*, *B. cylindrica*, and *R. apiculata*. The *A. marina* was the most frequently observed species at Gili Meno, known for its remarkable adaptability to saline and muddy environments. This adaptability is largely due to its unique pneumatophore root structure, resembling nails or pencils, which also aids in reducing coastal abrasion. The *A. marina* has a high tolerance for extreme conditions, including high salinity levels and muddy substrates. Its broad salinity tolerance allows it to thrive in environments with salinity levels as high as 90% (Suwanto et al. 2021). Muddy substrates, which are prevalent in Indonesia provide ideal conditions for growth of *Avicennia* and *Rhizophora* mangrove stands. Furthermore, the proximity of mangrove areas to saltwater lake on Gili Meno creates an optimal environment for *A. marina* to flourish. As noted by Chowdhury et al. (2022), *A. marina* is a salt-tolerant species that rapidly establishes itself in muddy coastal regions.

According to Figure 6, mangroves are depicted in bright red color within the imagery, a coloration that arises from their relatively high reflectance values in the Near-Infrared (NIR), Short-Wave Infrared (SWIR), and red bands, distinguishing them from other objects. This distinction is attributed to the sensitivity of NIR and red bands to vegetation greenness, as highlighted by Wang et al. (2018). Additionally, Sadeghi et al. (2015), emphasized that SWIR bands serve as sensitive indicators of soil moisture levels, a crucial factor in mangrove habitats influenced by tidal dynamics.

Based on Figure 7, the mangrove area in Gili Meno was detected to be around 6.88 ha. This represents a reduction of 5.02 hectares compared to 11.9 ha reported by Rahman and Hadi (2021), highlighting a potential decline due to anthropogenic activities. However, accurate and extensive information on the area of mangrove vegetation in Gili Meno remains limited.

Referring to Table 3, the highest AGC value was recorded at point 7, amounting to 190.40 ton/ha, while the lowest was at point 1, with a value of 41.23 ton/ha. The average AGC across 10 points was 103.16 ton/ha. For comparison, Suardana et al. (2023) found an average AGC of 82.97 tons/ha in Benoa Bay, Bali, while Rijal et al. (2023) reported an average AGC of 57.16 ton/ha in Loh Buaya, Komodo National Park. In contrast, Hoa et al. (2023) documented an AGC of 344.97 ton/ha in mangroves in Tien Yen District, Quang Ninh Province, and Aye et al. (2023) reported an average AGC of 100.34±50.70 Mg C ha^{-1} in the mangroves of Ayeyarwady Region, Myanmar. Comparatively, Wicaksono et al. (2016) found an average AGC of 21.64 ton/ha on the island of Karimun Jawa, which is notably lower than the findings of current study. The variations in AGC values are directly influenced by the mangrove biomass within each plot. Biomass represents a primary form of carbon storage, derived from the process of photosynthesis. A positive correlation exists between trunk diameter and biomass, where a greater DBH signifies an older tree with higher carbon reserves (Purnamasari et al. 2020). In this study, DBH values ranged from 1.3 cm to 28.3 cm, with the highest average DBH found in the dominant species, *A. marina*, at 8.8 cm. Similarly, Suardana et al. (2023) revealed that the highest AGC value, reaching 175.77 ton/ha, was observed in plots dominated by the *Rhizophora mucronata*, a species characterized by a substantial average DBH of 28.85 cm.

Based on Figure 8, the IRECI index exhibited the strongest correlation with an R^2 value of 0.76 (Table 4). The red edge band is particularly sensitive to various biophysical parameters of vegetation, making highly effective in detecting vegetation index values, as demonstrated by Zhu et al. (2017). Its presence in Sentinel-2 imagery allows for the detailed assessment of vegetation health, as noted by Goswami et al. (2021). Vegetation with high chlorophyll content absorbs more energy within the 670-760 nm spectrum, a phenomenon explained by Curran et al. (1995). Positioned between the red and NIR bands in the electromagnetic spectrum, the red edge represents a

critical spectral region characterized by a rapid change in vegetation reflectance (Suardana et al. 2023). In this study, the vegetation indices such as mRE-SR and CIR also utilize the red edge band, but exhibit slightly lower R^2 values, with 0.71 for both, compared to IRECI. However, these indices still demonstrate a good relationship with AGC. The variation in R^2 values is likely due to differences in how the red edge is utilized within each index. For example, IRECI, employs the red edge 2 and NIR bands, which individually achieved R^2 values of 0.59 for red edge 2 and 0.60 for NIR, the highest among all other bands. This suggests that the red edge 2 and NIR bands play a significant role in influencing in mangrove carbon estimation. Moreover, vegetation indices like NDVI, TRVI, and OSAVI, which are constructed using combinations of the NIR and red bands, also showed strong R^2 values of 0.73, 0.76, and 0.73, respectively. Vegetation indices that incorporate green, red, red-edge, and NIR channels are particularly sensitive to plant chlorophyll content (Daughtry et al. 2000; Haboudane et al. 2002). Wicaksono et al. (2016) found that the DVI vegetation index, due to its simple formula and reliance on the NIR band, is highly effective for above ground carbon stock mapping. Similarly, Zhou et al. (2020) found that vegetation indices derived from the combination of red and NIR band accurately estimating leaf chlorophyll content. The red spectral band effectively captures chlorophyll, while the NIR band exhibits significant reflectivity, contributing to the strong performance of these indices (Suardana et al. 2022).

According to Table 5, the green band and red edge 1 band were the only ones that did not exhibit a significant relationship with AGC. The blue, red, and SWIR bands demonstrated relatively weak correlations with AGC. In contrast, the red edge 2, red edge 3, and NIR bands showed strong correlations with AGC, with commendable R^2 values and relatively low RMSE values, indicating their significant role in explaining variation in AGC. However, band 3 and red edge 1 had very low R^2 values, suggesting they were ineffective in this study's model. The decision to use vegetation indices derived from the red edge and NIR bands was informed by their effectiveness in vegetation detection, as noted by Nguy-Robertson et al. (2014) and Imran et al. (2020). Differentiating vegetation indices into those incorporating the red edge band and those that do not provide alternative for estimating AGC using optical satellite images that lack red edge bands (e.g., Landsat, SPOT, Planet Scope). However, incorporating the red edge band into AGC estimation shows promise for achieving enhanced results. As emphasized by Sibanda et al. (2015) and Dube et al. (2018), the red edge and NIR bands have robust correlations with biomass, making them foundational for AGC calculations. Looking ahead, expanding the application of the red edge band to all optical satellite images could drive further advancements in AGC estimation.

The model developed in this study, based on IRECI index derived from the Sentinel-2 imagery, demonstrated significant accuracy in predicting Above Ground Ccarbon (AGC). The model's predicted and observed AGC values produced an R^2 value of 0.76, with a prediction error of 17.14 tons per hectare. These findings show an improvement in accuracy compared to previous studies, such as Wicaksono et al. (2016), who reported an R2 value of 0.69 using multispectral imagery in Karimun Jawa, Indonesia, and Hidayah et al. (2024), who reported an R^2 value of 0.63 using Sentinel-1 SAR data in Bali, Indonesia. However, the R^2 value achieved in this study is lower than that reported by Hati et al. (2024), who obtained an R^2 value of 0.97 using ALOS PALSAR-2 images in India, Candra et al. (2016), who achieved R^2 value of 0.85 using WorldView-2 image data in Bali, Indonesia, and Mariano et al. (2024), who reported R^2 value of 0.90 using Landsat-8 in Brazil. This difference in R^2 values may be attributed to the variations in imagery and the limited coverage of mangrove areas in some data collection plots of this study, which resulted in insufficient pixel representation in the Sentinel-2 imagery (see Figure 12). The unique environment of mangrove habitat in Gili Meno, surrounded by land and interspersed with other tropical vegetation encircling a saltwater lake, may also contribute to the suboptimal R^2 values observed in this study. Additionally, the limited sample size may have further affected the R^2 values. Despite these limitations, Sentinel-2 data proved effective in predicting mangrove carbon content in small areas. To improve accuracy, future research should aim to expand the dataset and consider using a combination of red edge bands, which are known for their sensitivity in detecting vegetation density.

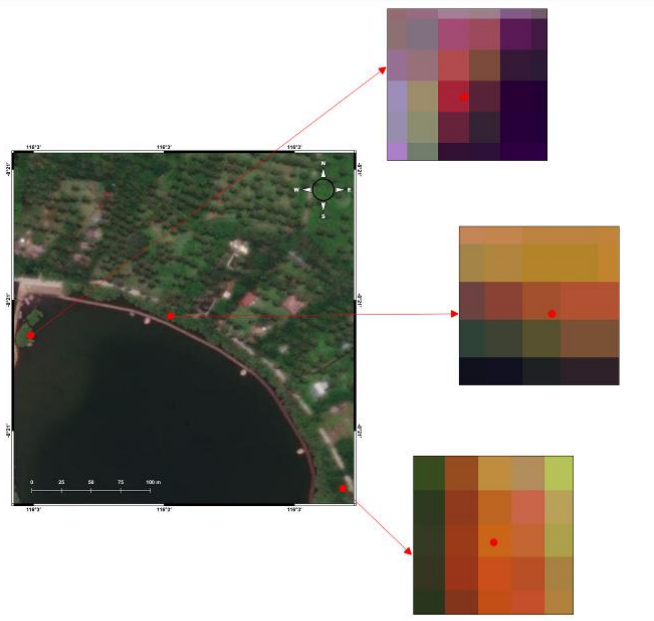

Figure 12. Some points of Gili Meno, West Nusa Tenggara, Indonesia, mangrove area in sentinel pixel

In conclusion, the mangroves in Gili Meno face significant challenges due to rapid tourism development and waste accumulation, which have led to a considerable decline in their extent and health. This study found *A. marina* to be the predominant species in the area, demonstrating remarkable adaptability to the saline and muddy conditions of Gili Meno. The assessment revealed variations in Above Ground Carbon (AGC) values, with an average of 103.16 ton/ha. The IRECI index, utilizing red edge and NIR bands, was found to be the most accurate in predicting AGC, with an R^2 value of 0.76. Despite the environmental complexity and small sample size, Sentinel-2 data has shown promise in effectively estimating mangrove carbon content. Expanding data collection and exploring combined use of red edge bands needs to be further explored for enhancing prediction accuracy, contributing to better mangrove conservation and management strategies.

ACKNOWLEDGEMENTS

The author would like to express his appreciation for the collaboration and assistance provided by the Korea-Indonesia MTCRC (Marine Technology Cooperation Research Center) and *Balai Kawasan Konservasi Perairan Nasional Kupang Wilayah Kerja* TWP Gili Matra, Indonesia. This research is financially supported through the Joint Agreement between the Korea-Indonesia MTCRC and the Faculty of Marine Science and Fisheries, Universitas Udayana, Indonesia under Research Grant 2023 No: 25/MTCRC/VII/2023; B/1/UN14.2.13/HK.07.01/2023.

REFERENCES

Akhiat Y, Manzali Y, Chahhou M, Zinedine A. 2021. A new noisy random forest based method for feature selection. Cybern Inf Technol 21 (2): 10-28. DOI: 10.2478/cait-2021-0016.

Alam M, Zafar S, Muhammad W. 2017. Assessment of Sentinel-2 vegetation indices for plot level tree AGB estimation. Intl Conf Aerosp Sci Eng 2017: 8374278. DOI: 10.1109/icase.2017.8374278.

As-syakur AR, Aryunisha PEP, Wijana IMS, Novanda IGA, Dewi IGAIP, Andiani AAE, Premananda MG, Sugiana IP. 2023. Comparison of mangrove canopy covering accuracy using Landsat 8 and Landsat 9 imagery based on several vegetation indices in West Bali National Park. E3S Web Conf 442: 03001. DOI: 10.1051/e3sconf/202344203001.

Aye WN, Tong X, Li J, Tun AW. 2023. Assessing the carbon storage potential of a young mangrove plantation in Myanmar. Forests 2023 14: 824. DOI: 10.3390/f14040824.

Baloloy AB, Blanco AC, Ana RRCS, Nadaoka K. 2020. Development and application of a new Mangrove Vegetation Index (MVI) for rapid and accurate mangrove mapping. ISPRS J Photogramm Remote Sens 166: 95-117. DOI: 10.1016/j.isprsjprs.2020.06.001.

Bindu G, Rajan P, Jishnu ES, Ajith Joseph K. 2020. Carbon stock assessment of mangroves using remote sensing and geographic information system. Egypt J Remote Sens Space Sci 23 (1): 1-9. DOI: 10.1016/j.ejrs.2018.04.006.

Blackburn GA. 1998. Quantifying chlorophylls and caroteniods at leaf and canopy scales: An evaluation of some hyperspectral approaches. Remote Sens Environ 66 (3): 273-285. DOI: 10.1016/S0034-4257(98)00059-5.

Candra ED, Hartono, Wicaksono P. 2016. Above ground carbon stock estimates of mangrove forest using Worldview-2 imagery in Teluk Benoa, Bali. IOP Conf Ser: Earth Environ Sci 47: 012014. DOI: 10.1088/1755-1315/47/1/012014.

Chowdhury A, Naz A, Dasgupta R, Maiti SK. 2022. Blue carbon: Comparison of chronosequences from *Avicennia marina* plantation and *Proteresia coarctata* dominated mudflat, at the world's largest mangrove wetland. Sustainability 15 (1): 368. DOI: 10.3390/su15010368.

Curran PJ, Windham WR, Gholz HL. 1995. Exploring the relationship between reflectance red edge and chlorophyll concentration in slash pine leaves. Tree Physiol 15 (3): 203-206. DOI: 10.1093/treephys/15.3.203.

Dan TT, Chen CF, Chiang SH, Ogawa S. 2016. Mapping and change analysis in mangrove forest by using Landsat imagery. ISPRS Ann Photogramm Remote Sens Spat Inf Sci III–8: 109-116. DOI: 10.5194/isprsannals-iii-8-109-2016.

Daughtry CS, Walthall CL, Kim MS, De Colstoun EB, McMurtrey III JE. 2000. Estimating corn leaf chlorophyll concentration from leaf and canopy reflectance. Remote Sens Environ 74 (2): 229-239. DOI: 10.1016/S0034-4257(00)00113-9.

Dinilhuda A, Akbar AA, Herawaty H. 2020. Potentials of mangrove ecosystem as storage of carbon for global warming mitigation. Biodiversitas 21 (11): 5353-5362. DOI: 10.13057/biodiv/d211141.

Dong S, Chen Z, Gao B, Guo H, Sun D, Pan Y. 2020. Stratified even sampling method for accuracy assessment of land use/land cover classification: A case study of Beijing, China. Intl J Remote Sens 41 (16): 6427-6443. DOI: 10.1080/01431161.2020.1739349.

Dube T, Gara TW, Mutanga O, Sibanda M, Shoko C, Murwir A, Hatendi CM. 2018. Estimating forest standing biomass in savanna woodlands as an indicator of forest productivity using the new generation WorldView-2 sensor. Geocarto Intl 33 (2): 178-188. DOI: 10.1080/10106049.2016.1240717.

Fadaei H, Suzuki R, Sakai T, Torii K. 2012. A proposed new vegetation index, the Total Ratio Vegetation Index (TRVI), for arid and semi-arid regions. Intl Arch Photogramm Remote Sens Spat Inf Sci XXXIX-B8: 403-407. DOI: 10.5194/isprsarchives-xxxix-b8-403-2012.

Fourqurean JW, Johnson B, Kauffman JB, Kennedy H, Lovelock CE, Megonigal JP, Rahman A, Saintilan N, Simard M. 2019. Coastal Blue Carbon. Habitat Conservation, Ci, 860. http://www.habitat.noaa.gov/coastalbluecarbon.html.

Giri C, Ochieng E, Tieszen LL, Zhu Z, Singh A, Loveland T, Masek J, Duke N. 2011. Status and distribution of mangrove forests of the world using earth observation satellite data. Global Ecol Biogeogr 20 (1): 154-159. DOI: 10.1111/j.1466-8238.2010.00584.x.

Gitelson AA, Shashi BV, Andreas V, Donald CR, Galina K, Bryan L, Timothy JA, George GB, Andrew ES. 2003. Novel technique for remote estimation of CO_2 flux in maize. Geophys Res Lett 30 (9): 1486. DOI: 10.1029/2002GL016543.

Goswami J, Das R, Sarma KK, Raju PN. 2021. Red Edge Position (REP), an indicator for crop stress detection: Implication on rice (*Oryza sativa* L). Int J Environ Clim Chang 11 (4): 88-96. DOI: 10.9734/ijecc/2021/v11i430396.

Haboudane D, Miller JR, Tremblay N, Zarco-Tejada PJ, Dextraze L. 2002. Integrated narrow-band vegetation indices for prediction of crop chlorophyll content for application to precision agriculture. Remote Sens Environ 81 (2-3): 416-426. DOI: 10.1016/S0034-4257(02)00018-4.

Hati JP, Mukhopadhyay A, Chaube NR, Hazra S, Pramanick N, Gupta K, Bharadwaz GSVSA, Mitra D. 2024. Estimation of above ground biomass with Synthetic Aperture Radar (SAR) data in Lothian Island, Sundarbans, India. J Indian Soc Remote Sens 52(4): 757-769. DOI: 10.1007/s12524-023-01788-9.

Hickey SM, Callow NJ, Phinn S, Lovelock CE, Duarte CM. 2018. Spatial complexities in aboveground carbon stocks of a semi-arid mangrove community: A remote sensing height-biomass-carbon approach. Estuar Coast Shelf Sci 200: 194-201. DOI: 10.1016/j.ecss.2017.11.004.

Hidayah Z, Utama RYS, As-Syakur AR, Rachman HA, Wiyanto DB. 2024. Mapping mangrove above ground carbon stock of Benoa Bay Bali using sentinel-1 satellite imagery. IOP Conf Ser Earth Environ Sci 1298 (1): 012013. DOI: 10.1088/1755-1315/1298/1/012013.

Hoa NH, Son HT, Linh NT, de Vicent DO, Linh NN. 2023. Using Planetscope data to estimate carbon sequestration of mangrove forests: A case study in Tien Yen District, Quang Ninh Province. J For Sci Technol 15: 87-99. DOI: 10.55250/jo.vnuf.2023.15.087-099.

Imran HA, Gianelle D, Rocchini D, Dalponte M, Martín MP, Sakowska K, Wohlfahrt G, Vescovo L. 2020. VIS-NIR, red-edge and NIR-shoulder based normalized vegetation indices response to co-varying leaf and canopy structural traits in heterogeneous grasslands. Remote Sensing 12 (14): 2254. DOI: 10.3390/rs12142254.

Indonesian National Standard (SNI). 2011. Pengukuran dan Perhitungan Cadangan Karbon– Pengukuran Lapangan untuk Penaksiran Cadangan Karbon Hutan (Ground Based Forest Carbon Accounting). Badan Standardisasi Nasional, Jakarta. [Indonesian]

Iqbal MH. 2020. Valuing ecosystem services of Sundarbans mangrove forest for improved conservation: Approach of randomized conjoint experiment. For Econ Rev 2 (1): 117-132. DOI: 10.1108/fer-04 2020-0008.

Kauffman JB, Donato DC. 2012. Protocols for the Measurement, Monitoring and Reporting of Structure, Biomass and Carbon Stocks in Mangrove Forests. Working Paper 86. CIFOR, Bogor, Indonesia.

KKP. 2020. Ecosystem ATP Gili Matra. Marine and Fisheries of Republic Indonesia p.2443. [Indonesian]

Komiyama A, Poungparn S, Kato S. 2005. Common allometric equations for estimating the tree weight of mangroves. J Trop Ecol 21 (4): 471-477. DOI: 10.1017/S0266467405002476.

Kristensen E, Bouillon S, Dittmar T, Marchand C. 2008. Organic carbon dynamics in mangrove ecosystems: A review. Aquat Bot 89 (2): 201-219. DOI: 10.1016/j.aquabot.2007.12.005.

Kumar L, Mutanga O. 2017. Remote sensing of above-ground biomass. Remote Sens 9 (9): 935. DOI: 10.3390/rs9090935.

Liu L, Dong Y, Huang W, Du X, Ren B, Huang L, Zheng Q, Ma H. 2020. A disease index for efficiently detecting wheat fusarium head blight using sentinel-2 multispectral imagery. IEEE Access 8: 52181-52191. DOI: 10.1109/ACCESS.2020.2980310.

Mariano NM, da Silva JB, de Brito HC. 2024. Carbon stock estimation in a Brazilian mangrove using optical satellite data. Environ Monit Assess 196 (1): 9. DOI: 10.1007/s10661-023-12151-3.

Maurya K, Mahajan S, Chaube N. 2021. Remote sensing techniques: Mapping and monitoring of mangrove ecosystem—A review. Complex Intell Syst 7 (6): 2797-2818. DOI: 10.1007/s40747-021-00457-z.

Murdiyarso D, Purbopuspito J, Kauffman JB et al. 2015. The potential of Indonesian mangrove forests for global climate change mitigation. Nat Clim Chang 5 (12): 1089-1092. DOI: 10.1038/NCLIMATE2734.

Nguy-Robertson AL, Peng Y, Gitelson AA et al. 2014. Estimating green LAI in four crops: Potential of determining optimal spectral bands for a universal algorithm. Agric For Meteorol 192-193: 140-148. DOI: 10.1016/j.agrformet.2014.03.004.

Pham TD, Yoshino K, Le NN, Bui DT. 2018. Estimating aboveground biomass of a mangrove plantation on the Northern coast of Vietnam using machine learning techniques with an integration of ALOS-2 PALSAR-2 and Sentinel-2A data. Intl J Remote Sens 39 (22): 7761-7788. DOI: 10.1080/01431161.2018.1471544.

Purnamasari E, Kamal M, Wicaksono P. 2020. Relationship analysis of vegetation structural properties and the aboveground carbon stock of mangrove forest. E3S Web Conf 200: 02020. DOI: 10.1051/e3sconf/202020002020.

Purnamasari E, Kamal M, Wicaksono P. 2021. Comparison of vegetation indices for estimating above-ground mangrove carbon stocks using PlanetScope image. Reg Stud Mar Sci 44: 101730. DOI: 10.1016/j.rsma.2021.101730.

Rahman FA, Hadi AP. 2021. Kandungan C-organik substrat ekosistem mangrove di danau air asin Gili Meno Kabupaten Lombok Utara. Bioscientist 9 (2): 516-526. DOI: 10.33394/bioscientist.v9i2.4276. [Indonesian]

Ramdani F, Rahman S, Giri C. 2018. Principal polar spectral indices for mapping mangroves forest in South East Asia: study case Indonesia. Intl J Digit Earth 12 (10): 1103-1117. DOI: 10.1080/17538947.2018.1454516.

Rijal SS, Pham TD, Noer'Aulia S, Putera MI, Saintilan N. 2023. Mapping mangrove above-ground carbon using multi-source remote sensing data and machine learning approach in Loh Buaya, Komodo National Park, Indonesia. Forests 14 (1): 94. DOI: 10.3390/f14010094.

Rondeaux G, Steven M, Baret F. 1996. Optimization of soil-adjusted vegetation indices. Remote Sens Environ 55 (2): 95-107. DOI: 10.1016/0034-4257(95)00186-7.

Rouse J, Haas R, Schell J, Deering D. 1973. Monitoring vegetation systems in the great plains with ERTS. Proc Earth Resour Technol Satell Symp 1: 309-317.

Sadeghi M, Jones SB, Philpot WD. 2015. A linear physically-based model for remote sensing of soil moisture using short wave infrared bands. Remote Sens Environ 164: 66-76. DOI: 10.1016/j.rse.2015.04.007.

Saragi-Sasmito MF, Murdiyarso D, June T, Sasmito SD. 2018. Carbon stocks, emissions, and aboveground productivity in restored secondary tropical peat swamp forests. Mitig Adapt Strateg Glob Chang 24: 521-533. DOI: 10.1007/s11027-018-9793-0.

She B, Yang Y, Zhao Z, Huang L, Liang D, Zhang D. 2020. Identification and mapping of soybean and maize crops based on Sentinel-2 data. Intl J Agric Biol Eng 13 (6): 171-182. DOI: 10.25165/j.ijabe.20201306.6183.

Sibanda M, Mutanga O, Rouget M. 2015. Examining the potential of Sentinel-2 MSI spectral resolution in quantifying above ground biomass across different fertilizer treatments. ISPRS J Photogramm Remote Sens 110: 55-65. DOI: 10.1016/j.isprsjprs.2015.10.005.

Simarmata N, Wikantika K, Tarigan TA, Aldyansyah M, Tohir RK, Fauziah A, Purnama Y. 2021. Analisis transformasi indeks NDVI, NDWI dan SAVI untuk identifikasi kerapatan vegetasi mangrove menggunakan citra Sentinel di Peisisir Timur Provinsi Lampung. Jurnal Geografi 19 (2): 69-79. DOI: 10.26740/jggp.v19n2.p69-79. [Indonesian]

Suardana AAMAP, Anggraini N, Nandika MR Aziz K, As-syakur AR, Ulfa A, Wijaya AD, Prasetio W, Winarso G, Dimyati RD. 2023. Estimation and mapping above-ground mangrove carbon stock using Sentinel-2 data derived vegetation indices in Benoa Bay of Bali Province, Indonesia. For Soc 7 (1): 116-134. DOI: 10.24259/fs.v7i1.22062.

Suardana AMAP, Anggraini N, Aziz K, Nandika MR, Ulfa A, Wijaya AD, As-syakur AR, Winarso G, Prasetio W, Dewanti R. 2022. Biomass estimation model and carbon dioxide sequestration for mangrove forest using Sentinel-2 in Benoa Bay, Bali. Intl J Remote Sens Earth Sci 19 (1): 91-100. DOI: 10.30536/j.ijreses.2022.v19.a3797

Suwa R, Rollon R, Sharma S, Yoshikai M, Albano GMG, Ono K, Adi NS, Ati RNA, Kusumaningtyas MA, Kepel TL, Maliao RJ, Primavera-Tirol YH, Blanco AC, Nadaoka K. 2021. Mangrove biomass estimation using canopy height and wood density in the South East and East Asian regions. Estuar Coast Shelf Sci 248: 106937. DOI: 10.1016/j.ecss.2020.106937.

Suwanto A, Takarina ND, Koestoer RH, Frimawaty E. 2021. Diversity, biomass, covers, and ndvi of restored mangrove forests in Karawang and Subang coasts, West Java, Indonesia. Biodiversitas 22 (9): 4115-4122. DOI: 10.13057/biodiv/d220960.

Wahyuni S, Haerani H, Mursalim M, Azizan FA. 2024. The use of Sentinel-2 vegetation indices imagery in detecting the effect of plant distance to the productivity of corn crops. BIO Web Conf 96: 05001. DOI: 10.1051/bioconf/20249605001.

Wang B, Jia K, Liang S, Xie X, Wei X, Zhao X, Yao Y, Zhang X. 2018. Assessment of Sentinel-2 MSI spectral band reflectances for estimating fractional vegetation cover. Remote Sens 10 (12): 1927. DOI: 10.3390/rs10121927.

Wicaksono P, Danoedoro P, Hartono, Nehren U. 2016. Mangrove biomass carbon stock mapping of the Karimunjawa Islands using multispectral remote sensing. Intl J Remote Sens 37 (1): 26-52. DOI: 10.1080/01431161.2015.1117679.

World Agroforestry Center. 2022. http://db.worldagroforestry.org/wd

Worthington TA, Andradi-Brown DA, Bhargava R et al. 2020. Harnessing big data to support the conservation and rehabilitation of mangrove forests globally. One Earth 2 (5): 429-443. DOI: 10.1016/j.oneear.2020.04.018.

Zhang T, Lin W. 2014. Metal–organic frameworks for artificial photosynthesis and photocatalysis. Chem Soc Rev 43 (16): 5982-5993. DOI: 10.1039/C4CS00103F.

Zheng H, Cheng T, Li D, Zhou X, Yao X, Tian Y, Cao W, Zhu Y. 2018. Evaluation of RGB, color-infrared and multispectral images acquired from unmanned aerial systems for the estimation of nitrogen accumulation in rice. Remote Sens 10 (6): 824. DOI: 10.3390/rs10060824.

Zhou X, Zhang J, Chen D, Huang Y, Kong W, Yuan L, Ye H, Huang W. 2020. Assessment of leaf chlorophyll content models for winter wheat using Landsat-8 multispectral remote sensing data. Remote Sens 12 (16): 2574. DOI: 10.3390/rs12162574.

Zhu Y, Liu K, Liu L, Myint SW, Wang S, Liu H, He Z. 2017. Exploring the potential of world view-2 red-edge band-based vegetation indices for estimation of mangrove leaf area index with machine learning algorithms. Remote Sens 9 (10): 1060. DOI: 10.3390/rs9101060.